AAPS PharmSciTech, Vol. 9, No. 2, June 2008 (© 2008)
DOI: 10.1208/s12249-008-9081-5

Research Article

Crystal Structure Determination of New Antimitotic Agent Bis(*p*-fluorobenzyl) trisulfide

Haoyun An,[1,3] Xiurong Hu,[2] Jianming Gu,[2] Linshen Chen,[2] Weiming Xu,[2] Xiaopeng Mo,[1] Wanhong Xu,[1] Xiaobo Wang,[1] and Xiao Xu[1]

Received 20 November 2007; accepted 7 March 2008; published online 22 April 2008

Abstract. The purpose of this research was to investigate the physical characteristics and crystalline structure of bis(*p*-fluorobenzyl)trisulfide, a new anti-tumor agent. Methods used included X-ray single crystal diffraction, X-ray powder diffraction (XRPD), Fourier-transform infrared (FT-IR) spectroscopy, differential scanning calorimetric (DSC) and thermogravimetric (TG) analyses. The findings obtained with X-ray single crystal diffraction showed that a monoclinic unit cell was a=12.266(1) Å, b=4.7757 (4) Å, c=25.510(1) Å, β=104.25(1)°; cell volume=1,448.4(2) Å^3, Z=4, and space group $C2/c$. The XRPD studies of the four crystalline samples, obtained by recrystallization from four different solvents, indicated that they had the same diffraction patterns. The diffraction pattern stimulated from the crystal structure data is in excellent agreement with the experimental results. In addition, the identical FT-IR spectra of the four crystalline samples revealed absorption bands corresponding to S–S and C–S stretching as well as the characteristic aromatic substitution. Five percent weight loss at 163.3 °C was observed when TG was used to study the decomposition process in the temperature range of 20–200 °C. DSC also allowed for the determination of onset temperatures at 60.4(1)–60.7(3) °C and peak temperatures at 62.1(3)–62.4 (3) °C for the four crystalline samples studied. The results verified that the single crystal structure shared the same crystal form with the four crystalline samples investigated.

KEY WORDS: antimitotic agent; fluorapacin; single crystal structure; thermal analysis; XRPD.

INTRODUCTION

The novel pharmacophores discovered from natural sources (1–3) have been playing an important role for modern drug discovery in combination with computer-aid drug design, combinatorial and medicinal chemistry efforts (4–8). Over 50% of the anticancer drugs currently used are either natural products or derived from natural products (9,10). The clinical successes of taxanes, alkaloids and other types of natural products promoted us to search for new medicines from natural sources (11,12). Dibenzyl trisulfide has been recently discovered as a new antitumor lead compound (13,14), and it was isolated from a subtropical shrub *Petiveria alliacea L.*, a member of *Phytolaccaceae* family (15). The herb medicine Anamu or Apacin, prepared from *Petiveria alliacea*, has been used in Caribbean, Latin America, West Africa and other regions for hundreds of years to treat pains, flu, inflammation, tumor, bacteria, fungi and other diseases (16). This initial lead was further optimized to an advanced lead, bis(*p*-fluorobenzyl)trisulfide, which exhibits broad cellular antitumor activities (13,14). Systematic preclinical studies of bis(*p*-fluorobenzyl)trisulfide at ACEA Biosciences provided an investigational new drug (IND) candidate, fluorapacin, as an antimitotic agent.

Fluorapacin is a small molecule natural product derivative and represents a new and unique structural series (Fig. 1). The structure of fluorapacin has been elucidated by UV-VIS, MS, ^{1}H, ^{13}C and ^{19}F NMR spectroscopic and combustion analyses (13). A drug with identical composition may have different physical properties and stability, which could also affect the bioavailability, efficacy and toxicity profiles (17–20). Since the properties of the solid state for a given drug may be extremely relevant for its quality, the International Conference of Harmonization (ICH) requires a polymorphic study for new active pharmaceutical ingredients (APIs; 21). Therefore, further crystal structure determination is still critical to develop fluorapacin into a new antitumor medicine. The structural characterization of drug substances by X-ray diffraction plays a central role during the development of pharmaceuticals (17–20,22–24). Single crystal X-ray diffraction provides detail structural information, while X-ray powder diffraction is a powerful tool in identifying different crystal phases and verifying the equivalence of different crystallines based on their unique diffraction patterns. The simulated diffraction, established based on the single crystal structure information, can be used to verify and support a specific powder diffraction pattern of a drug as being truly representative of a single phase (18). Therefore, it is important to investigate the solid-state properties and structure of

[1] ACEA Biosciences, Inc., 6779 Mesa Ridge Road, Suite 100, San Diego, CA 92121, USA.
[2] Analytical and Measurement Center of Zhejiang University, 38 Zheda Road, Hangzhou, 310027, China.
[3] To whom correspondence should be addressed. (e-mail: han@aceabio.com)

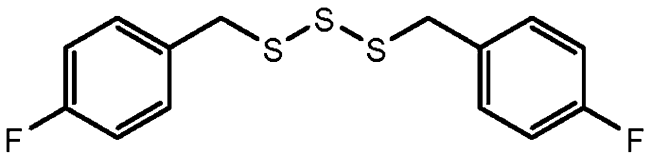

Fig. 1. Chemical structure of bis(*p*-fluorobenzyl)trisulfide, fluorapacin

fluorapacin, and ultimately verify the stable solid-state form for the development and approval of this new drug.

At present, the crystal structure of the drug candidate fluorapacin was characterized by X-ray single crystal diffraction. The spectroscopic and thermal properties of crystalline fluorapacin were studied by differential scanning calorimetry (DSC), thermogravimetry (TG) and infrared spectroscopic analyses. The different crystallines obtained from different solvents were further investigated using X-ray powder diffraction to warrant the therapeutic and safety profiles of fluorapacin. The combined results obtained utilizing these thermal analytical and crystallographic technologies verified the high quality, single phase of drug substance fluorapacin.

MATERIALS AND METHODS

The batch L0014 bis(*p*-fluorobenzyl)trisulfide, fluorapacin, was synthesized with an HPLC purity of 99.86% according to our reported procedure (13), and was used for the preparation of single crystal and other crystalline samples through recrystallization from different solvents. Solvents were used as purchased without further purification. Fluorapacin was recrystallized from anhydrous ethanol, *n*-hexane, ethyl acetate and acetone providing white crystalline samples 14-1, 14-2, 14-4 and 14-6, respectively. These samples were used for FT-IR, differential scanning calorimetry, thermogravimetry and X-ray powder diffraction (XRPD) studies.

Slow evaporation of the solvent from a solution of fluorapacin in anhydrous ethanol provided colorless single crystals. A colorless crystal with approximate dimensions of 0.50×0.37×0.11 mm was measured using an area detector on a Rigaku R-AXIS-RAPID diffractometer with graphite monochromated Mo-Kα radiation (λ=0.71069 Å). A total of 6656 data points were collected, of which 1,655 were unique. Data reduction was performed with CrystalStructure (25). The crystal structure was solved with direct methods using SIR97 (26) program and refined on $F^{2'}$s anisotropically by a full-matrix, least-squares method using the CRYSTALS program (27). Anisotropic displacement parameters for non-hydrogen atoms were applied. Hydrogen atoms were placed at the metrically calculated positions and were refined isotropically using a riding mode. The results show that the crystal belongs to monoclinic with a space group of *C* 2/c, having cell parameters *a*=12.266(1) Å, *b*=4.7757(4) Å, *c*=25.510(1) Å, beta=104.25(1)°, and *Z*=4. The final results were *R*1=0.0311 [I>2(I)], *wR*=0.0851 (for all data), the goodness of fit ref=1.010 with a shift/su max=0.0000, the remnants density max=0.35 and min=−0.30.

The X-ray powder diffraction spectra were collected on a Rigaku D/Max-2500 powder diffractometer, using CuKα (λ for Kα=1.54059 Å) radiation at 40 kV and 200 mA. The scans were run from 3.0 to 50.0° 2θ, with an increasing step size of 0.02° and counting time duration of 0.5 s for each step. Data were processed using the MDI-Jade version 7.0 software.

Table I. Bond Distances and Angles for Fluorapacin

Parameter			
Bond distances (Å, angstrom)			
S1–S2	2.046 (1)	S1–C7	1.821 (1)
F1–C1	1.367 (2)	C1–C2	1.346 (4)
C1–C6	1.356 (3)	C2–C3	1.388 (2)
C3–C4	1.383 (2)	C4–C5	1.379 (2)
C4–C7	1.499 (2)	C5–C6	1.386 (2)
C2–H2	0.930	C3–H3	0.930
C5–H5	0.930	C6–H6	0.930
C7–H71	0.970	C7–H72	0.970
Bond angles (°)			
S2–S1–C7	102.8 (1)	S1–S2–S1[a]	104.6 (1)
F1–C1–C2	118.6 (2)	F1–C1–C6	118.3 (2)
C2–C1–C6	123.2 (2)	C1–C2–C3	118.3 (2)
C2–C3–C4	121.0 (2)	C3–C4–C5	118.2 (1)
C3–C4–C7	120.9 (1)	C5–C4–C7	120.8 (1)
C4–C5–C6	121.0 (2)	C1–C6–C5	118.3 (2)
S1–C7–C4	114.6 (1)	C1–C2–H2	120.8
C3–C2–H2	120.8	C2–C3–H3	119.5
C4–C3–H3	119.5	C4–C5–H5	119.5
C6–C5–H5	119.5	C1–C6–H6	120.8
C5–C6–H6	120.8	S1–C7–H71	108.2
S1–C7–H72	108.2	C4–C7–H71	108.2
C4–C7–H72	108.2	H71–C7–H72	109.5

Note: [a] 1−*x*, *y*, 0.5−*z*

Melting points were measured using an X-6 microscopic melting point apparatus. FT–IR spectra were recorded from potassium bromide disks prepared with each crystalline sample on a VECTOR–22 FT-IR spectrophotometer in the scan range of 4,000–400 cm^{-1}. Approximately 4–7 mg powder samples of 14-1, 14-2, 14-4 and 14-6 were used for differential scanning calorimetry (DSC) and thermogravimetry (TG) analyses. The DSC analysis was performed on a TA DSC Q100 differential scanning calorimeter at the heating rate of 10 °C /min under a nitrogen flow of 50 cm^3 /min. A temperature range of 35–100 °C was scanned. The DSC temperature axis was calibrated in an aluminum pan with indium standard sample (melting point 156.6 °C, heat of fusion 28.45 J/g). The samples were equilibrated at 25 °C and heated to 300 °C at a heating rate of 10 °C/min under a nitrogen flow

Table II. Crystallographic Information for Fluorapacin

Parameter	Data
Chemical formula	C_{14} H_{12} F_2 S_3
Formula weight	314.43
Crystal system	Monoclinic
Space group	*C* 2/c
a	12.266 (1) Å
b	4.7757 (4) Å
c	25.510 (1) Å
β	104.25(1)°
V	1,448.4(2) $Å^3$
Z	4
Calculated density	1.442 $g \cdot cm^{-3}$
Absorption coefficient	0.515 mm^{-1}
R indices (all data)	*R*1=0.0311, *wR*2=0.0851
Goodness of fit	1.010
Largest diff. peak and hole	0.30 $e^-/Å^3$ and −0.35 $e^-/Å^3$

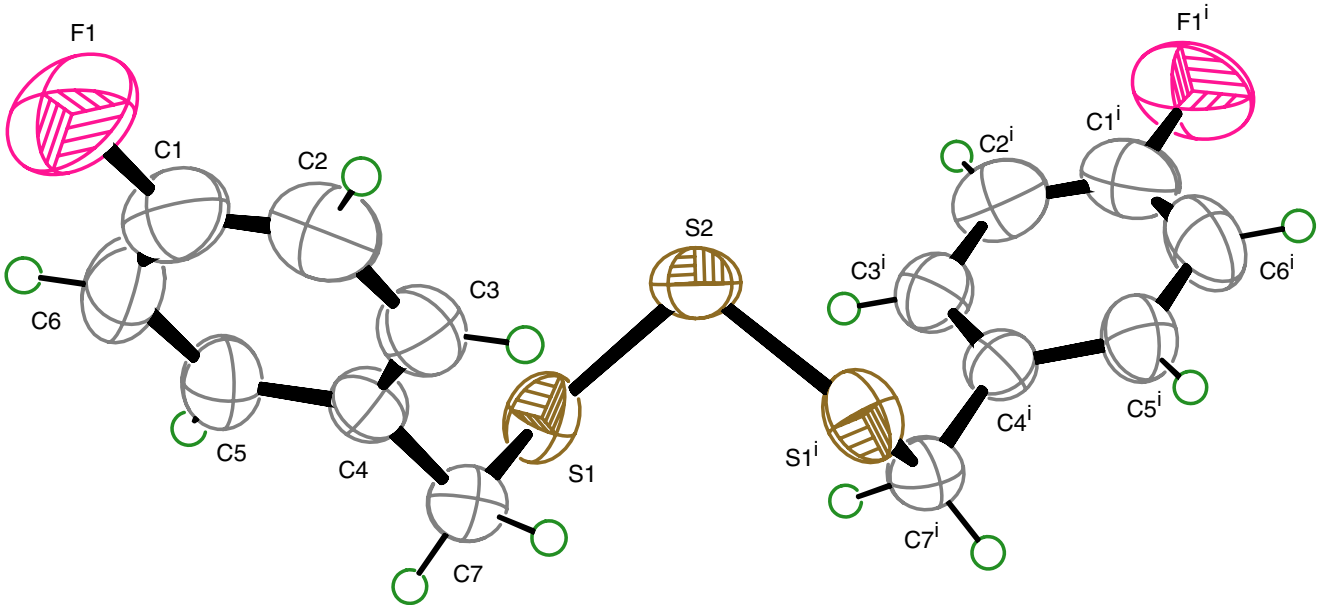

Fig. 2. The molecular configuration and atom-numbering scheme of fluorapacin. Displacement ellipsoids are drawn at the 50% probability level. H atoms are drawn as spheres of arbitrary radius

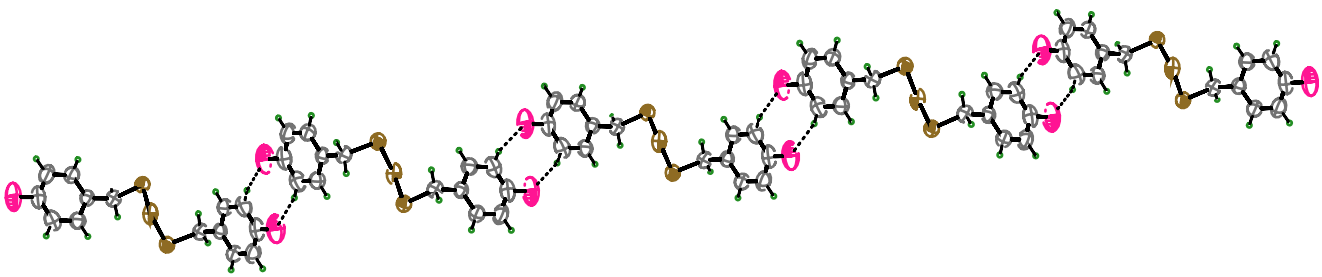

Fig. 3. Intermolecular interactions (*dashed line*) in a chain of molecules

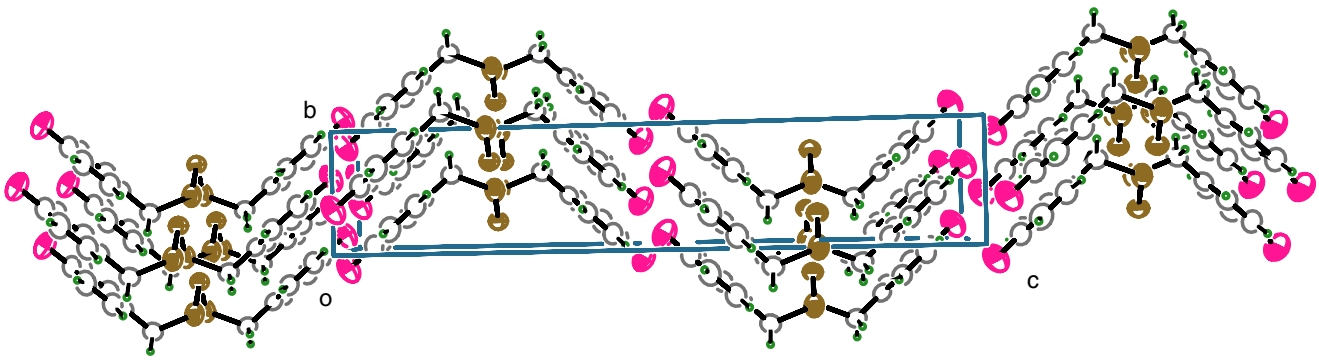

Fig. 4. Packing diagram of fluorapacin projected along *c* axis

of 50 cm^3/min. The calibrated temperature accuracy was ±0.02 °C, and the calorimetric accuracy for the heat of fusion was ±0.11%. The thermogravimetry (TG) analyses were conducted with a TA SDT Q600 thermogravimetric analyzer at the heating rate of 10 °C/min under a nitrogen flow of 120 cm^3/min. A temperature range of 20–200 °C was scanned. The TG temperature axis was calibrated in alumina pans with standard samples indium (melting point 156.6 °C), zinc (melting point 419.5 °C) and gold (melting point 1,063 °C) for three temperature points. The samples were equilibrated at 25 °C and heated to 1,200 °C at a heating rate of 10 °C/min under a nitrogen flow of 120 cm^3/min. The calibrated temperature accuracy was ±1.5 °C. Standard α-Al_2O_3 poises were used for weight calibration, and the weighing accuracy was ±0.05%.

RESULTS AND DISCUSSION

Crystal Structure and XRPD

The structure of fluorapacin (Fig. 1) has been characterized by various spectroscopic and elemental analyses (13). The crystal structure of fluorapacin was determined by X-ray single crystal diffraction. The structural parameters and crystallographic information for fluorapacin are listed in Tables I and II. The ORTEP (28) drawings are shown in Figs. 2, 3, 4. Fluorapacin crystallizes in the centrosymmetric space group *C*2/c. There is one half of a molecule in the asymmetric unit. The central sulfur atom S2, located at x= 0.500, y=0.233 and z=0.250, is a symmetric center of the molecule (Fig. 2). The bond angle of S1–S2–S1[i] (i symmetric code: $1-x$, y, $1/2-z$) is 104.6(1)°. Atoms S1 and S2 deviate from the phenyl plane, and the torsion angle of C4–C7–S1–S2 is 73.01(14)°. Two phenyl rings in the molecule are almost perpendicular to each other, forming a dihedral angel of 95.8 (3)° (Table II and Fig. 2). In the crystal, centrosymmetric dimers $R_2^2(8)$ (29) are formed through weak intermolecular interaction C2–H2....F1[ii] (ii symmetric code: $1/2-x$, $-1/2-y$, $-z$), linking the molecules into an infinite chain (Fig. 3). The molecules are aligned along the *c* axis and packed along the *b* axis, forming a ladder as shown in Fig. 4.

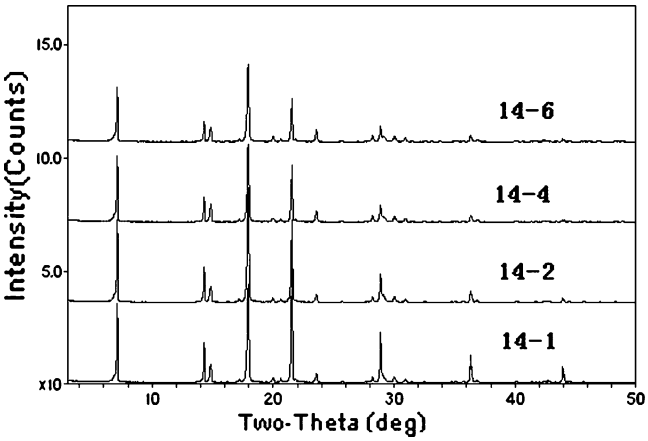

Fig. 5. X-ray powder diffraction patterns of fluorapacin samples crystallized from four different solvents. 14-1 (from ethanol), 14-2 (from *n*-hexane), 14-4 (from ethyl acetate), 14-6 (from acetone)

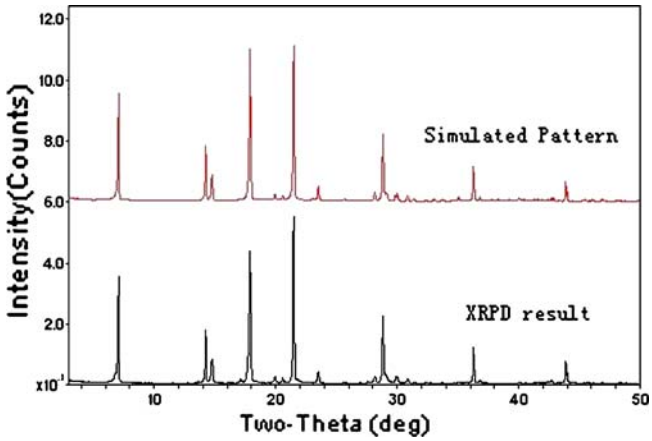

Fig. 6. Comparison of simulated and experimental X-ray powder diffraction patterns

X-ray powder diffraction (XRPD) represents the most reliable methodology for the crystallographic characterization of drug substances. Powder diffraction can generally be used to verify the equivalence of different crystalline samples by their fingerprint type of unique diffraction patterns. The powder diffraction studies of fluorapacin indicated that the four crystalline samples obtained from four different solvents had nearly identical characteristic diffraction pattern (Fig. 5), and showed an identical morphological form for the tested crystalline samples. The crystal structure information obtained was utilized to further verify the conclusions obtained from powder diffraction results. Therefore, the single crystal sample, used for X-ray single crystal diffraction studies, was used for further X-ray powder diffraction investigation. The powder diffraction pattern is shown in Fig. 6 (bottom diffractogram). The crystal structure data obtained from the X-ray single crystal diffraction was used to calculate the diffraction pattern (see top pattern in Fig. 6). The results clearly indicated that the experimental XRPD pattern (bottom diffractogram, Fig. 6) was nearly identical as those of other samples (Fig. 5). In addition, it is also in an excellent agreement with the simulated diffraction pattern (top pattern, Fig. 6) calculated based on crystal structure data.

FT-IR Spectrometry, Differential Scanning Calorimetry and Thermogravimetry

The crystalline samples 14-1, 14-2, 14-4 and 14-6 were also studied utilizing infrared spectroscopic, DSC and TG analytical methods to understand the physical and thermal properties of fluorapacin. These crystalline samples have nearly identical appearance and melting point (see Table III). Their infrared spectra are identical in the range of 4,000–400 cm^{-1} (Fig. 7). The strong absorption band at 1,234 cm^{-1} shows the $\upsilon_{C\text{-}F}$ stretching. The bands at 1,602 and 1,513 cm^{-1} represent the $\upsilon_{C=C}$ skeletal vibration. The in-plane deformation $\delta_{=CH}$ at 1,157 cm^{-1} verified the 1,4-disubstituted benzene ring. The out-of-plane deformation band $\delta_{=CH}$ at 833 cm^{-1} represents the two adjacent hydrogen atoms on the benzene ring, which further verified the *para*-substitution. The bands at 652 and 462 cm^{-1} are characteristic $\upsilon_{C\text{-}S}$ and $\upsilon_{S\text{-}S}$ stretching vibrations. The structure of fluorapacin was confirmed by these characteristic

Table III. Melting Point and DSC Data of Fluorapacin Crystalline Samples

Sample number	Solvent used for crystallization	m. p. (°C)	DSC onset temperature (°C)	DSC peak temperature (°C)
14–1	Anhydrous ethanol	61.4~62.2	60.6 (1)	62.1 (3)
14–2	*n*-Hexane	61.4~62.4	60.7 (1)	62.1 (2)
14–4	Ethyl acetate	61.5~62.5	60.6 (4)	62.4 (1)
14–6	Acetone	61.5~62.2	60.7 (3)	62.4 (3)

absorption bands. These crystalline samples are expected to have the same crystalline form.

The four crystalline samples of fluorapacin obtained from different solvents were analyzed by differential scanning calorimetry (DSC) and thermogravimetry (TG) to evaluate their thermal properties. The DSC diagrams of the samples in 35–100 °C exhibited an endothermic peak at the melting temperature (Table III, Fig. 8). Their onset temperature ranged from 60.6–60.7 °C, and the endothermic peak temperature, ranged as 62.1–62.4 °C. The melting point data was confirmed by using a melting point apparatus (Table III). Except for the endothermic peak corresponding to the melting temperature, the DSC diagrams did not show other thermal events due to possible loss of solvent, oxidative degradation or other phase transition processes. All four samples provided nearly identical TG diagrams in the 20–200 °C range although they showed low thermal stability with about 5% weight loss at 163.3 °C. Figure 8 shows the representative DSC and TG diagrams of the crystalline sample 14–1 obtained from ethanol. Other three samples, 14-2, 14-4 and 14-6, showed nearly identical DSC and TG diagrams (Data not shown). Therefore, the DSC and TG analyses indicated that the four crystalline samples, from different solvents, had the same thermal properties and were not solvated.

CONCLUSIONS

Based on the physical and spectroscopic properties, thermal analyses, and X-ray powder diffraction results obtained above, it was concluded that the four crystalline samples of fluorapacin obtained from four different solvents represented the same crystal form of fluorapacin, and the crystal structure of this stable crystal form was also verified by X-ray crystallography. Therefore, the crystalline form of the drug substance fluorapacin should provide reliable and consistent results during development studies of this new antimitotic agent. These

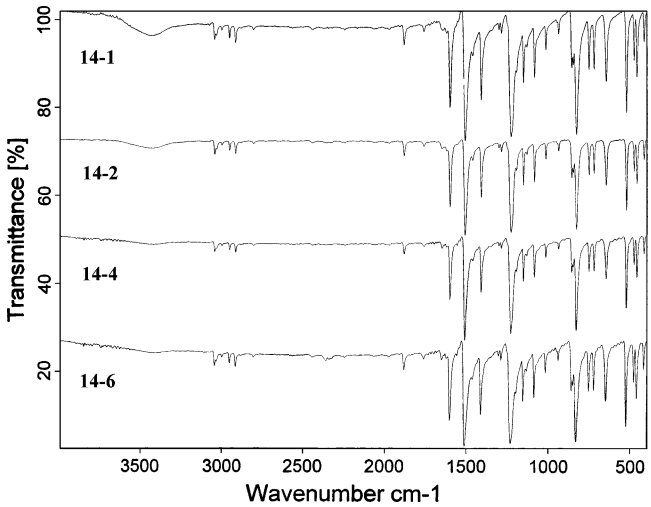

Fig. 7. Solid-state infrared spectra of fluorapacin crystalline samples 14-1, 14-2, 14-4 and 14-6 (in the order *from top to bottom*)

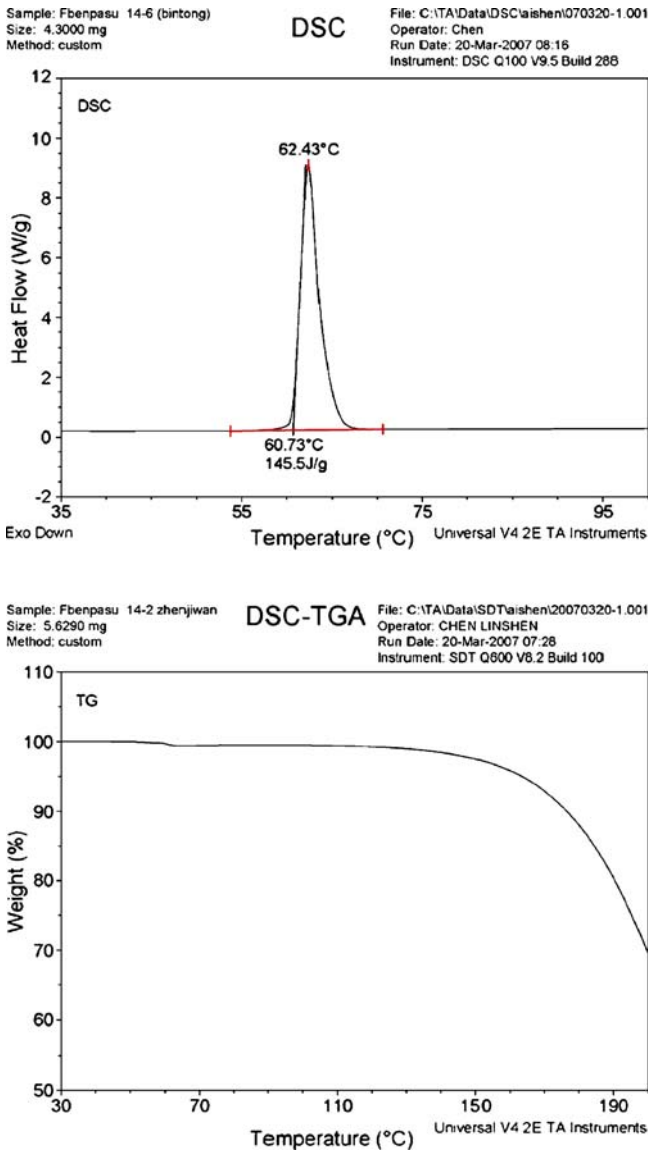

Fig. 8. Typical DSC and TG diagrams of fluorapacin (crystalline 14-1 from ethanol)

findings provide confidence for the further development of fluorapacin as a potential antimitotic drug.

REFERENCES

1. D. J. Newman, G. M. Gragg, and K. M. Snader. Natural products as sources of new drugs over the period 1981–2002. *J. Nat. Prod.* **66**:1022–1037 (2003).
2. P. K. Lai, and J. Roy. Antimicrobial and chemopreventive properties of herbs and spices. *Curr. Med. Chem.* **11**:1451–1460 (2004).
3. D. J. Newman, and G. M. Gragg. Marine natural products and related compounds in clinical and advanced preclinical trials. *J. Nat. Prod.* **67**:1216–1238 (2004).
4. Y. W. Chin, M. J. Balunas, H. B. Chai, and A. D. Kinghorn. Drug discovery from natural sources. *The AAPS PharmSciTech.* **8**: E239–E253 (2006).
5. G. M. Cragg, and D. J. Newman. A tale of two tumor targets: Topoisomerase I and tubulin. The Wall and Wani contribution to cancer chemotherapy. *J. Nat. Prod.* **67**:232–244 (2004).
6. B. G. Livett, K. R. Gayler, and Z. Khalil. Drug from the sea: Conopeptides as potential therapeutics. *Curr. Med. Chem.* **11**:1715–1723 (2004).
7. J. G. Topliss, A. M. Clark, E. Ernst, C. D. Hufford, G. A. R. Johnston, J. M. Rimoldi, and B. J. Weimann. Natural and synthetic substances related to human health. *Pure. Appl. Chem.* **74**:1957–1985 (2002).
8. K. H. Lee. Anticancer drug design based on plant-derived natural products. *J. Biomed. Sci.* **6**:236–250 (1999).
9. N. Darwiche, S. El-Banna, and H. Gali-Muhtasib. Cell cycle modulatory and apoptotic effects of plant-derived anticancer drugs in clinical use or development. *Expert. Opin. Drug. Discov.* **2**:361–379 (2007).
10. M. Liscovitch, and Y. Lavie. Cancer multidrug resistance: A review of recent drug discovery research. *Idrugs.* **5**:349–355 (2002).
11. G. Petrangolini, G. Cassinelli, G. Pratesi, *et al.* Antitumour and antiangiogenic effects of IDN 5390, a novel C-seco taxane, in a paclitaxel-resistant human ovarian tumour xenograft. *British J. Cancer.* **90**:1464–1468 (2004).
12. D. Polizzi, G. Pratesi, M. Tortoreto, R. Supino, A. Riva, E. Bombardelli, and F. Zunino. A novel taxane with improved tolerability and therapeutic activity in a panel of human tumor xenografts. *Cancer Res.* **59**:1036–1040 (1999).
13. H. An, J. Zhu, X. B. Wang, and X. Xu. Synthesis and antitumor evaluation of new trisulfide derivatives. *Bioorg. Med. Chem. Lett.* **16**:4826–4829 (2006).
14. X. Xu, H. An, X. B. Wang, inventers. Substituted organosulfur compounds and methods of using thereof. *PCT /WO* 2005/112933. December 1, 2005; *United States Patent Application* 2005/0261321. November 24, 2005; *Chinese Patent application* 200580012460.5. November 17, 2006.
15. J. R. de Sousa, A. J. Demuner, J. A. Pinheiro, E. Breitmaier, and B. K. Cassels. Dibenzyl trisulphide and *trasn-N*-methyl-4-methoxyproline from *Petiveria alliacea*. *Phytochem.* **29**:3653–3655 (1990).
16. Tropical Plant Database–Anamu (Petiveria alliacea). http://www.rain-tree.com/anamu.htm (accessed 12/20/07).
17. E. Tedesco, D. Giron, and S. Pfeffer. Crystal structure elucidation and morphology study of pharmaceuticals in development. *CrystEngComm.* **4**:393–400 (2002).
18. G. A. Stephenson. Applications of X-ray powder diffraction in the pharmaceutical industry. *The Rigaku J.* **22**:2–15 (2005).
19. C. R. Gardner, C. T. Walsh, and O. Almarsson. Drugs as materials: Valuing physical form in drug discovery. *Nature Rev. Drug Discov.* **3**:926–934 (2004).
20. Y. Lv, Y. S. Wu, and Q. T. Zheng. The application progress of X-ray diffraction analysis technique in new drug and pharmacy research. *Modern Instrument.* **3**:6–9 and 19 (2004).
21. United States Pharmacopoeial Convention. X-Ray Diffraction, General test <941>. United States Pharmacopoeia, 25th ed., Rockville, MD, 2002, pp. 2088–2089.
22. R. E. Dinnebier, P. Sieger, H. Nar, K. Shankland, and W. I. F. David. Structural characterization of three crystalline modifications of telmisartan by single crystal and high-resolution X-ray powder diffraction. *J. Pharm. Sci.* **89**:1465–1479 (2000).
23. S. L. Morissette, O. Almarsson, M. L. Peterson, *et al.* High-throughput crystallization: polymorphs, salts, co-crystals and solvates of pharmaceutical solids. *Adv. Drug. Deliv. Rev.* **56**:275–300 (2004).
24. A. R. Sheth, and D. J. W. Grant. Relationship between the structure and properties of pharmaceutical crystals. *Kona.* **23**:36–48 (2005).
25. Rigaku /MSC (2004). Crystal Structure. Version 3.60. Rigaku/MSC, 9009 New Trails Drive, The Woodlands, TX 77381-5209, USA.
26. A. Altomare, M. Burla, M. Camalli, *et al.* SIR 97: A new tool for crystal structure determination and refinement. *J. Appl. Cryst.* **32**:115–119 (1999).
27. P. W. Betteridge, J. R. Carruthers, R. L. Cooper, K. Prout, and D. J. Watkin. CRYSTALS version 12: Software for guided crystal structure analysis. *J. Appl. Cryst.* **36**:1487 (2003).
28. L. J. Farrugia. *ORTEP*-3 for Windows—a version of *ORTEP*-III with a Graphical User Interface (GUI). *J. Appl. Cryst.* **30**:565 (1997).
29. M. C. Etter. Encoding and decoding hydrogen-bond patterns of organic compounds. *Acc. Chem. Res.* **23**:120–126 (1990).